Title

Observation of ultralong valley lifetime in WSe_2/MoS_2 heterostructures.

Journal

Science advances, 3(7)

ISSN

2375-2548

Authors

Kim, Jonghwan
Jin, Chenhao
Chen, Bin
et al.

Publication Date

2017-07-01

DOI

10.1126/sciadv.1700518

Peer reviewed

SPINTRONICS

Observation of ultralong valley lifetime in WSe_2/MoS_2 heterostructures

Jonghwan Kim,[1,2]* Chenhao Jin,[1]* Bin Chen,[3] Hui Cai,[3] Tao Zhao,[1] Puiyee Lee,[1] Salman Kahn,[1] Kenji Watanabe,[4] Takashi Taniguchi,[4] Sefaattin Tongay,[3] Michael F. Crommie,[1,5,6] Feng Wang[1,5,6]†

The valley degree of freedom in two-dimensional (2D) crystals recently emerged as a novel information carrier in addition to spin and charge. The intrinsic valley lifetime in 2D transition metal dichalcogenides (TMD) is expected to be markedly long due to the unique spin-valley locking behavior, where the intervalley scattering of the electron simultaneously requires a large momentum transfer to the opposite valley and a flip of the electron spin. However, the experimentally observed valley lifetime in 2D TMDs has been limited to tens of nanoseconds thus far. We report efficient generation of microsecond-long-lived valley polarization in WSe_2/MoS_2 heterostructures by exploiting the ultrafast charge transfer processes in the heterostructure that efficiently creates resident holes in the WSe_2 layer. These valley-polarized holes exhibit near-unity valley polarization and ultralong valley lifetime: We observe a valley-polarized hole population lifetime of more than 1 μs and a valley depolarization lifetime (that is, intervalley scattering lifetime) of more than 40 μs at 10 K. The near-perfect generation of valley-polarized holes in TMD heterostructures, combined with ultralong valley lifetime, which is orders of magnitude longer than previous results, opens up new opportunities for novel valleytronics and spintronics applications.

INTRODUCTION

Atomically thin layers of semiconducting transition metal dichalcogenides (TMDs) exhibit unique electronic band structure (*1*, *2*) and fascinating physical properties (*3*, *4*). A pair of degenerate direct bands are present at the K and K′ points in the momentum space of hexagonal TMD monolayers, giving rise to a new valley degree of freedom known as the valley pseudospin (*5*, *6*). The strong spin-orbital coupling present in TMDs further locks the valley pseudospin to specific electron and hole spins for electronic states close to the bandgap (*5*, *6*). These coupled spin and valley degrees of freedom in TMDs can open up new ways to encode and process information for valleytronics, and they can be controlled flexibly through optical excitation, electrostatic gating, and heterostructure stacking. In particular, the spin-valley locking suggests that the intrinsic valley lifetime can be extremely long because a change of valley pseudospin requires a rare event with a large momentum transfer (from K to K′ valley) and an electron spin flip at the same time.

Tremendous progress has been made in exploring the valley pseudospin of two dimensional (2D) TMDs, ranging from optical generation and detection of valley polarization (*7*–*9*) to manipulation of valley pseudospin state with optical and magnetic field (*10*–*14*) and observation of the valley Hall effect (*15*). However, many challenges still exist for potential valleytronics applications. Chief among them is the relatively short valley lifetime. It was recently shown both theoretically and experimentally that the valley lifetime of excitons in TMD monolayers is severely constrained by the electron-hole exchange interaction through the Maialle-Silva-Sham mechanism (*16*–*20*), which can annihilate an exciton in one valley and create another exciton in the other valley (that is, depolarize the valley pseudospin) within picoseconds. However, the valley pseudospin of individual electrons or holes is not affected by this mechanism and can have a much longer lifetime. Photoinduced valley polarization of resident carriers in TMD monolayers is reported to have a much longer valley lifetime (*21*–*23*). The bright interlayer exciton in type II van der Waals heterostructure of TMDs provides another way to achieve a longer valley lifetime, where electrons and holes are separated into different layers and the electron-hole exchange interaction is strongly suppressed. However, experimentally observed valley lifetime for either resident carriers in TMD monolayers or indirect excitons in TMD heterostructures has been limited to a few tens of nanoseconds thus far (*21*–*24*). Here, we report efficient generation of ultralong-lived valley polarization in WSe_2/MoS_2 heterostructures. Using ultrafast pump-probe spectroscopy that covers the time scale from femtoseconds to microseconds, we show that perfectly valley-polarized holes can be generated in the WSe_2 layer within 50 fs because of the ultrafast charge transfer processes in the WSe_2/MoS_2 heterostructure (*25*, *26*). These valley-polarized holes exhibit a population decay lifetime of more than 1 μs and a depolarization lifetime (that is, intervalley scattering lifetime) of more than 40 μs at 10 K, which is orders of magnitude larger than previously reported values. The near-unity valley polarization and ultralong valley lifetime observed here will enable new ways to probe and manipulate valley and spin degrees of freedom in TMDs.

RESULTS

We investigate high-quality WSe_2/MoS_2 heterostructures using polarization-resolved pump-probe spectroscopy. Figure 1B shows the optical microscopy image of a representative WSe_2/MoS_2 heterostructure. The WSe_2 (encircled by the blue dashed line) and MoS_2 (encircled by the red dashed line) monolayers are first exfoliated mechanically from bulk crystals onto SiO_2/Si substrates and then stacked to form the heterostructure (denoted by the black dashed line) by a dry transfer method using a polyethylene terephthalate (PET) stamp (Supplementary Text). The heterostructure region can be visualized most strikingly

[1]Department of Physics, University of California, Berkeley, Berkeley, CA 94720, USA. [2]Department of Materials Science and Engineering, Pohang University of Science and Technology, Pohang 790-784, Korea. [3]School for Engineering of Matter, Transport and Energy, Arizona State University, Tempe, AZ 85287, USA. [4]National Institute for Materials Science, 1-1 Namiki, Tsukuba 305-0044, Japan. [5]Materials Sciences Division, Lawrence Berkeley National Laboratory, Berkeley, CA 94720, USA. [6]Kavli Energy NanoScience Institute, University of California, Berkeley and Lawrence Berkeley National Laboratory, Berkeley, CA 94720, USA.
*These authors contributed equally to this work.
†Corresponding author. Email: fengwang76@berkeley.edu

in the photoluminescence (PL) image (Fig. 1C), where the PL at the WSe_2 A-exciton resonance (1.65 eV at room temperature) is quenched by more than four orders of magnitude in the heterostructure region compared to the WSe_2-only region. This quenching of PL is a signature of the type II heterojunction in WSe_2/MoS_2 heterostructures, where the conduction band minimum and valence band maximum reside in the MoS_2 and WSe_2 layers, respectively, and an ultrafast charge transfer process takes the electron from the WSe_2 to the MoS_2 layer upon photoexcitation of WSe_2 excitons (Fig. 1A).

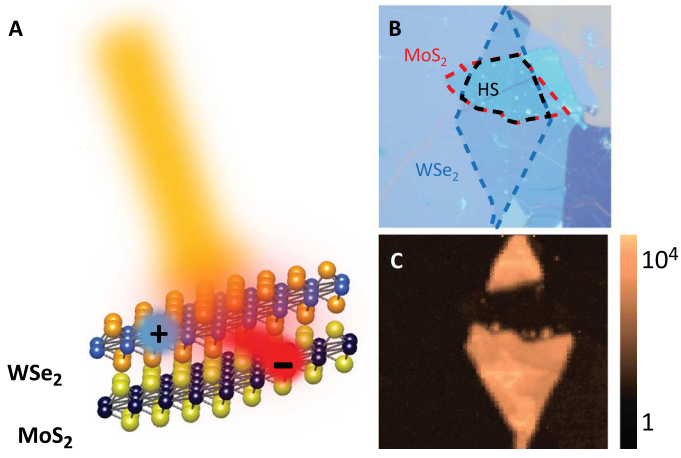

Fig. 1. Ultrafast charge transfer process in the WSe_2/MoS_2 heterostructure. (**A**) Illustration of the ultrafast electron transfer process in the WSe_2/MoS_2 heterostructure. The WSe_2/MoS_2 heterostructure forms a type II heterojunction where the conduction band minimum and the valence band maximum reside in MoS_2 and WSe_2, respectively. Photoexcited electrons transfer rapidly to the MoS_2 layer, whereas holes remain in the WSe_2 layer. (**B**) Optical microscope image of a representative WSe_2/MoS_2 heterostructure. Blue, red, and black dashed lines encircle WSe_2, MoS_2, and heterostructure (HS) regions, respectively. Scale bar, 10 μm. (**C**) PL image of the WSe_2/MoS_2 heterostructure at WSe_2 A-exciton resonance (1.65 eV) at room temperature. PL is quenched by four orders of magnitude in the heterostructure compared to the WSe_2-only region due to the ultrafast electron transfer process in the heterostructure.

The ultrafast electron transfer process in the heterostructure allows for efficient generation of valley-polarized holes in WSe_2, as illustrated in Fig. 2A: Resonant photoexcitation with left circularly polarized (LCP) light selectively creates electron-hole pairs (that is, excitons) at the K valley in the WSe_2 layer (encircled with dashed box). After the excitation, the electrons can transfer to the MoS_2 layer within 50 fs and leave behind resident holes in the K valley of the WSe_2 layer. These valley-polarized holes can exhibit ultralong lifetime: The population and valley polarization relaxation processes of resident holes, such as radiative recombination and exchange interaction (Maialle-Silva-Sham mechanism), are markedly suppressed because the holes are well-separated from the electrons in not only real space but also momentum space. Compared with the previously studied valley polarization of the bright interlayer exciton (which requires the presence of both electrons and holes), the lifetime of resident holes is not limited by the decay of the electrons in the other layer. To achieve the longest valley lifetime, we choose mechanically exfoliated and stacked WSe_2/MoS_2 heterostructures: The exfoliated TMD layers exhibit much higher quality and fewer defects compared with chemical vapor deposition grown samples, and the WSe_2/MoS_2 heterostructure features the largest band offset among all TMD combinations (*27*, *28*) such that the electrons and holes are well confined in separate layers.

We investigate the dynamic evolution of valley-polarized holes in the WSe_2 layer using polarization-resolved pump-probe spectroscopy. The LCP pump pulses generate valley-polarized holes in the WSe_2 layer. This valley imbalance leads to a difference in the optical absorption of the heterostructure for LCP and right circularly polarized (RCP) light close to the WSe_2 A-exciton resonance and can thereby be probed by pump-induced changes in the reflection contrast (RC) spectra of circularly polarized probe pulses. The dynamic evolution of the polarization-resolved ΔRC from femtosecond to microsecond was measured by combining a mechanical delay line (from femtoseconds to nanoseconds) and an electronic delay (from nanoseconds to microseconds).

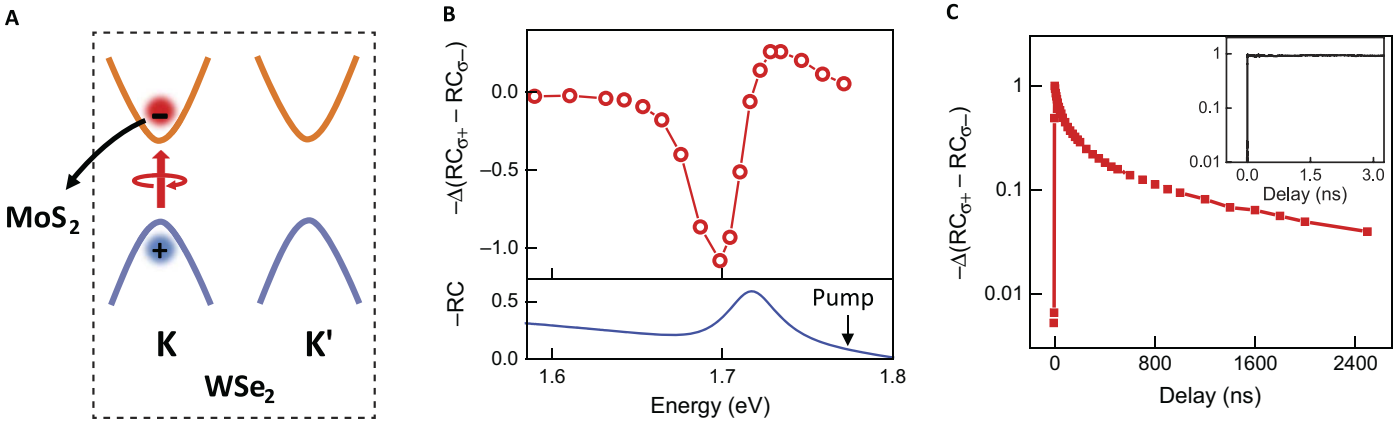

Fig. 2. Photoinduced CD signal of the WSe_2/MoS_2 heterostructure at 10 K. (**A**) Schematic of valley-polarized hole generation in the WSe_2 layer within the heterostructure. Upon photoexcitation with LCP light, excitons are resonantly created in the K valley of the WSe_2 layer (encircled with a dashed box). Ultrafast charge transfer process then efficiently transfers electrons to the MoS_2 layer and leaves resident holes at the K valley in the WSe_2 layer. (**B**) Top: Photoinduced CD spectrum at 3 ns. Bottom: RC spectrum of the WSe_2/MoS_2 heterostructure. RC spectrum is dominated by the optical absorption near the WSe_2 A-exciton resonance at 1.72 eV. The CD spectrum, $-\Delta(RC_{\sigma+} - RC_{\sigma-})$, shows prominent resonant feature near the WSe_2 A-exciton peak under LCP pump light at 1.78 eV (black arrow in the RC spectrum). (**C**) Decay dynamics of the resonant CD signal at 10 K. No decay is observed within 3.5 ns (inset). The decay curve over a longer time scale shows a significant slow decay component with a lifetime of more than 1 μs.

The top panel of Fig. 2B displays a photoinduced circular dichroism (CD) spectrum of the heterostructure probed at 3 ns after the pump excitation, and the bottom panel of Fig. 2B shows the RC spectrum of the heterostructure. The RC spectrum is dominated by the optical absorption near the WSe_2 A-exciton resonance peak at 1.72 eV (*29*, *30*). In the pump-probe study, we choose an excitation energy at 1.78 eV (black arrow in Fig. 2B) to selectively excite WSe_2 but not MoS_2 (which has an optical bandgap of 1.92 eV). In addition, pump excitation at this energy can provide full spectral information of the effect of resident holes on light absorption, as explained later. The CD signal is measured through $-\Delta(RC_{\sigma+} - RC_{\sigma-})$, which is the difference between the photoinduced changes in the RC of LCP ($RC_{\sigma+}$) and RCP ($RC_{\sigma-}$) light. The CD spectrum exhibits a prominent resonant feature around the A-exciton transition, and its magnitude is directly proportional to the valley-polarized hole density, that is, the difference between the hole density in the K valley (p_+) and K′ valley (p_-). The asymmetric derivative-like shape of the CD spectrum is analogous to the behavior observed in III-V and II-V semiconductor quantum wells (*31*, *32*), and it originates from the distinctive spectral response of LCP and RCP light to holes in a specific valley in WSe_2, which will be discussed later.

Figure 2C shows the time evolution of the CD signal with 1.71-eV probe photons at 10 K. The dynamic response from femtoseconds to nanoseconds is measured using a mechanical delay line, and it shows an almost constant CD signal from 300 fs to 3.5 ns (black curve in the inset). To capture the longer-term dynamics, we use an radio frequency (rf)–coupled diode laser synchronized to the femtosecond pulses to generate 3-ns-long probe pulses with electronically defined time delay up to a few microseconds (Supplementary Text). The CD signal from nanosecond to microsecond time scale is shown as red squares. Strikingly, the CD signal remains significant even after several microseconds, and the slowest decay component shows a lifetime of more than 1 μs (the relatively fast initial decay is largely due to interactions between photoexcited carriers; see pump fluence dependence in Supplementary Text). This microsecond lifetime of the valley-polarized hole density is orders of magnitude longer than that reported previously (*21*–*24*).

To separate the contributions from the population decay and the intervalley scattering to the overall lifetime of valley-polarized holes and quantify the degree of valley polarization upon optical initialization, we examine in more detail the dynamic behavior and spectrum dependence of the photoinduced valley polarization in WSe_2/MoS_2 heterostructures.

One key figure of merit in valley initialization and control is the degree of valley polarization, as defined by

$$P = \frac{p_+ - p_-}{p_+ + p_-}$$

where p_+ and p_- are hole densities in the K and K′ valleys, respectively. Here, we need to establish a quantitative relation between the hole density in a specific valley and the corresponding circularly polarized ΔRC spectra. Toward this goal, we analyze the photoinduced absorption changes in individual K and K′ valleys by separately examining the ΔRC spectra for LCP and RCP light. Figure 3 (A and B) shows the ΔRC spectra in the K and K′ valleys at 3 ns after resident holes are created in the K valley of WSe_2 through LCP light excitation. Distinctively different absorption changes are observed for the K valley ($\Delta RC_{\sigma+}$, black squares in Fig. 3A) and K′ valley ($\Delta RC_{\sigma-}$, red circles in Fig. 3B): The holes present in the K valley can modify further absorption at the K valley through a combination of the phase-space filling and Burstein-Moss effects, as previously observed for exciton states in quantum wells (*33*, *34*). It leads to a reduction of the exciton absorption oscillator strength accompanied by a slight blueshift of the exciton resonance. This is illustrated in the inset of Fig. 3A, where the original exciton absorption (black dashed line) is reduced and slightly blueshifted in the presence of the hole in the K valley (red solid line). Consequently, $\Delta RC_{\sigma+}$ for the K valley is dominated by an overall absorption reduction with a small absorption increase at the higher-energy side. However, the effect of K-valley holes on the absorption of the K′ valley is completely different because there is no Pauli blocking from phase-space filling. Instead, $\Delta RC_{\sigma-}$ is characterized by a decrease in the exciton absorption and an increase in the trion absorption due to the formation of an intervalley trion state (that is, exciton in the K′ valley and hole in the K valley), with the total absorption oscillator strength conserved. The inset in Fig. 3B further illustrates this process, where resident holes lead to oscillator strength transfer from exciton to intervalley trion absorption (red solid line) compared to the original spectrum (black dashed line).

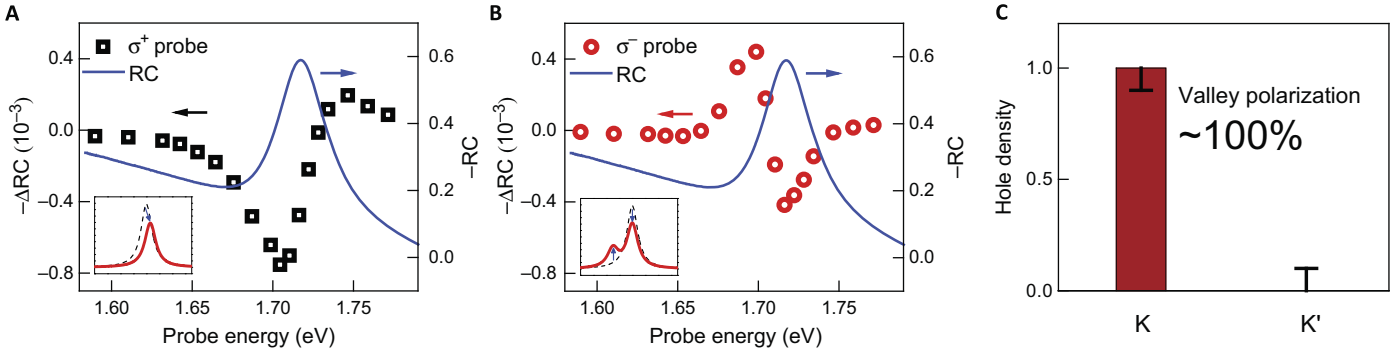

Fig. 3. An almost perfect valley polarization. (**A** and **B**) Resident holes in the K valley induce distinctively different absorption changes for the K (A) and K′ (B) valleys; RC of the heterostructure (blue solid line) is also shown for comparison. (A) The absorption change in the K valley features an overall reduction of the absorption oscillator strength and a slight blueshift of the exciton resonance. The inset illustrates the change of absorption spectrum, where the original exciton absorption (black dashed line) is modified in the presence of holes at the K valley (red solid line). This spectral change can be understood by the phase-space filling and Burstein-Moss effects. (B) The absorption change in the K′ valley shows a transfer of oscillator strength from exciton to trion absorption due to the formation of intervalley trions. However, the total oscillator strength is unaffected because there is no Pauli blocking effect. The inset illustrates the reduction of exciton absorption and emergence of intervalley trion absorption (red solid line) compared to the original spectrum (black dashed line). (**C**) The density of resident holes in the K and K′ valleys obtained by the integrated oscillator strength change of LCP and RCP light, which suggests near-perfect valley polarization (within 10% experimental uncertainty). The total hole density is normalized to 1.

The understanding that the holes present in one valley will reduce the overall optical absorption oscillator strength in the same valley but not the opposite valley allows for a direct experimental determination of hole population in each valley: p_+ and p_- are proportional to the integration of the ΔRC signal over frequency for LCP and RCP light, respectively. Following this approach, we find that an almost perfect valley polarization was created by the LCP excitation pulses: Holes exist only in the K valley but not in the K′ valley of WSe_2 within the experimental uncertainty (Fig. 3C). This efficient generation of valley-polarized holes presumably benefits from the ultrafast electron transfer process in the heterostructure, which separates the electrons and holes even before the valley depolarization of excitons produces a noticeable effect. Next, we quantitatively investigate the time evolution of valley-polarized holes. The decay of CD signal, which is proportional to the valley-polarized hole density (that is, $p_+ - p_-$), has two different contributions: (i) a population decay of the total hole density (that is, $p_+ + p_-$) and (ii) intervalley scattering that reduces the degree of valley polarization $P = (p_+ - p_-)/(p_+ + p_-)$. These two contributions can be obtained separately by examining the time evolution of $\Delta RC_{\sigma+} + \Delta RC_{\sigma-}$ and $(\Delta RC_{\sigma+} - \Delta RC_{\sigma-})/(\Delta RC_{\sigma+} + \Delta RC_{\sigma-})$, respectively.

Figure 4 (A and B) shows the photoinduced difference ($\Delta RC_{\sigma+} - \Delta RC_{\sigma-}$) and sum ($\Delta RC_{\sigma+} + \Delta RC_{\sigma-}$) signals at 3-, 80-, and 550-ns pump-probe delay. All the spectra are normalized to 1. Both the difference and sum spectra exhibit a constant profile around the A-exciton resonance (in the spectral range of 1.69 to 1.78 eV). In the sum response (Fig. 4B), a weak signal appears at around 1.66 eV over time, presumably due to some defect states that decay slowly. However, these defect states do not distinguish the K and K′ valleys and do not show any effect in the difference response (Fig. 4A). Because both the difference and sum spectra remain constant profiles within 1.69 to 1.78 eV, we can use a single probe photon energy at 1.71 eV to obtain the time evolution of the difference and sum signals, which characterize the difference and sum of hole densities in the K and K′ valleys, respectively.

Figure 4C displays the normalized decay dynamics of the total ($p_+ + p_-$, black dots) and valley-polarized ($p_+ - p_-$, red squares) hole densities in the heterostructure, as well as the degree of valley polarization (P, blue triangles). We found that the decay of valley-polarized holes ($p_+ - p_-$) is very similar to that of the total hole density ($p_+ + p_-$), indicating that the 1-μs decay lifetime observed in CD signals is dominated by a population

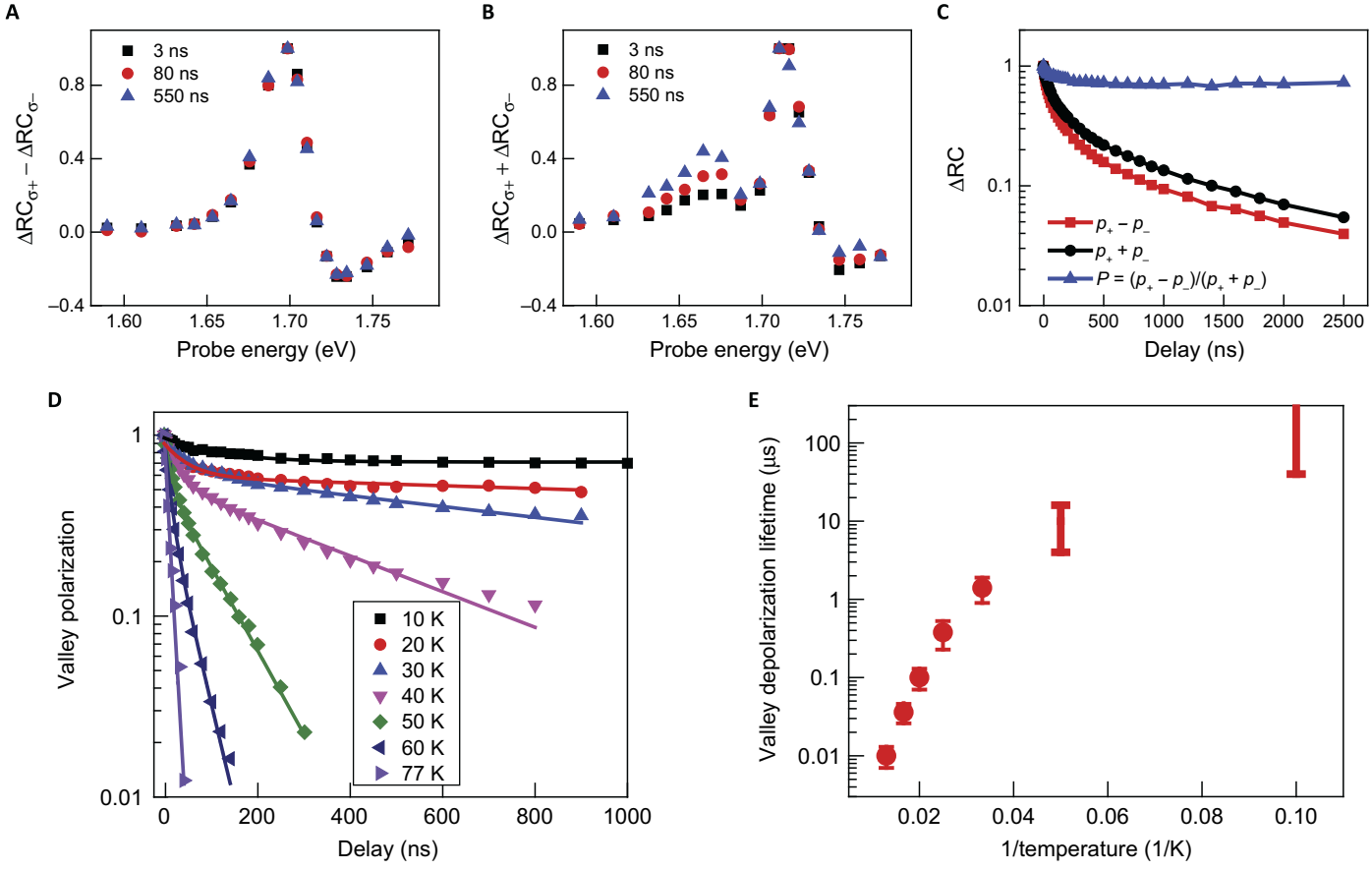

Fig. 4. Ultralong valley depolarization lifetime. (**A** and **B**) Photoinduced difference (A) and sum (B) responses of the two valleys at a pump-probe delay of 3 ns (black), 80 ns (red), and 550 ns (blue). All spectra were measured at 10 K and normalized to 1. Both the difference and sum spectra show constant profile over time, except for a weak signal at around 1.66 eV in the sum response due to some defect states that decay slowly. (**C**) Decay dynamics of the total hole population $p_+ + p_-$ (black dots), the valley-polarized hole population $p_+ - p_-$ (red squares), and the degree of valley polarization P (blue triangles) obtained with a probe energy of 1.71 eV. The decay of the valley-polarized hole population of ~1 μs is mainly due to the total population decay. However, the valley polarization does not show any apparent decay at 2.5 μs, corresponding to an ultralong valley depolarization lifetime approaching 40 μs. (**D**) Temperature-dependent decay dynamics of valley polarization from 10 to 77 K (symbols). Solid lines are biexponential decay fitting of experimentally measured decay dynamics, with decay lifetime of dominant slow components summarized in (**E**). The valley depolarization lifetime changes strongly with the temperature, suggesting an energy-activated mechanism in the intervalley hole scattering.

decay of holes. On the other hand, the valley depolarization lifetime from intervalley scattering is much longer: The degree of valley polarization does not show any apparent decay at 2.5 μs (except a small decrease within the first hundred nanoseconds). A conservative lower limit of the depolarization lifetime is 40 μs (Supplementary Text). However, there is significant uncertainty because of the minimal decay, and the upper limit can be many hundreds of microseconds.

At elevated temperatures, the valley depolarization becomes faster. Figure 4D shows the temperature dependence of the valley polarization decay. All decay curves show a weak fast component and a dominant slow component. We fit the measured decay dynamics (symbols in Fig. 4D) with a biexponential decay (solid lines) and focus on the behavior of the slow decay component. The slow depolarization lifetime changes from 10 ns at 77 K to above 40 μs at 10 K, as shown in Fig. 4E, which roughly follows an energy-activated type of dependence $\tau \sim e^{\frac{\Delta}{k_B T}}$, where k_B is the Boltzmann constant, with $\Delta \sim 20$ meV. A potential origin of the activation behavior in the temperature dependence is phonon-assisted intervalley scattering lifetime, which has been studied in systems, such as graphene and MoS_2 (*35*, *36*). The activation energy of ~20 meV matches with various phonon modes in WSe_2 at the K point (to satisfy the momentum conservation of intervalley scattering). In this sense, a phonon-assisted intervalley scattering, which is accompanied by spin-flipping through the Elliott-Yafet mechanism (Supplementary Text), can potentially account for the observed temperature dependence.

DISCUSSION

Our studies show that an almost perfect valley polarization of holes can be generated optically in WSe_2/MoS_2 heterostructures. The valley-polarized holes exhibit a population decay lifetime of ~ 1 μs and a depolarization lifetime of more than 40 μs at 10 K. Presumably, the population lifetime can be improved with better sample quality to reduce defect traps and with optimized heterostructure design to better separate the electrons and the holes. Therefore, a valley-polarized hole population with 40 μs should be possible. These valley-polarized holes are also spin-polarized because of the spin-valley locking in WSe_2. These long-lived valley and spin polarizations can open up new opportunities for valleytronics and spintronics applications based on 2D van der Waals heterostructures.

MATERIALS AND METHODS

Heterostructure preparation

WSe_2/MoS_2 heterostructures were prepared with PET stamp by dry transfer method (*37*). Monolayer WSe_2, MoS_2, and hexagonal boron nitride (hBN) flakes were first exfoliated onto the silicon substrate with a 90-nm oxide layer. We used PET stamp to pick up the hBN flake and monolayer MoS_2 in sequence. The PET stamp with hBN/MoS_2 was then stamped onto a monolayer WSe_2 flake to form a WSe_2/MoS_2 heterostructure. Polymer and samples were heated up to 60°C in the pickup and to 130°C in the stamp process. Finally, we dissolved the PET in dichloromethane for 12 hours at room temperature.

Generation of a nanosecond optical pulse with electronically controlled time delay

To generate optical pulses with electronically defined time delay, we first generated electronic pulses synchronized to the femtosecond laser. The femtosecond laser output (PHAROS, Light Conversion) had a repetition rate of 150 kHz defined by a regenerative amplifier, whose internal clock was used to trigger an electronic pulse generator (8082A, Hewlett-Packard). The output electronic pulse had a pulse duration of ~3 ns, which was then converted to optical pulses by an rf-coupled laser diode module (TCLDM9, Thorlabs). The relative time delay between the femtosecond laser output and the diode laser output could thereby be accurately controlled with the electronic delay in the pulse generator. The pulse duration of the nanosecond optical pulse was characterized by a fast photodiode and oscilloscope, from which we determined a pulse width of ~3 ns.

SUPPLEMENTARY MATERIALS

Supplementary material for this article is available at http://advances.sciencemag.org/cgi/content/full/3/7/e1700518/DC1

Supplementary Text

fig. S1. CD signal of the heterostructure at 10 K with different pump fluence from 65 to 650 nJ cm^{-2}.

Reference (*38*)

REFERENCES AND NOTES

1. A. Splendiani, L. Sun, Y. Zhang, T. Li, J. Kim, C. Y. Chim, G. Galli, F. Wang, Emerging photoluminescence in monolayer MoS_2. *Nano Lett.* **10**, 1271–1275 (2010).
2. K. F. Mak, C. Lee, J. Hone, J. Shan, T. F. Heinz, Atomically thin MoS_2: A new direct-gap semiconductor. *Phys. Rev. Lett.* **105**, 136805 (2010).
3. Q. H. Wang, K. Kalantar-Zadeh, A. Kis, J. N. Coleman, M. S. Strano,Electronics and optoelectronics of two-dimensional transition metal dichalcogenides. *Nat. Nanotechnol.* **7**, 699–712 (2012).
4. K. F. Mak, J. Shan, Photonics and optoelectronics of 2D semiconductor transition metal dichalcogenides. *Nat. Photonics* **10**, 216–226 (2016).
5. D. Xiao, G.-B. Liu, W. X. Feng, X. D. Xu, W. Yao, Coupled spin and valley physics in monolayers of MoS_2 and other group-VI dichalcogenides. *Phys. Rev. Lett.* **108**, 196802 (2012).
6. X. Xu, W. Yao, D. Xiao, T. F. Heinz, Spin and pseudospins in layered transition metal dichalcogenides. *Nat. Phys.* **10**, 343–350 (2014).
7. K. F. Mak, K. He, J. Shan, T. F. Heinz, Control of valley polarization in monolayer MoS_2 by optical helicity. *Nat. Nanotechnol.* **7**, 494–498 (2012).
8. T. Cao, G. Wang, W. Han, H. Ye, C. Zhu, J. Shi, Q. Niu, P. Tan, E. Wang, B. Liu, J. Feng, Valley-selective circular dichroism of monolayer molybdenum disulphide. *Nat. Commun.* **3**, 887 (2012).
9. H. Zeng, J. Dai, W. Yao, D. Xiao, X. Cui, Valley polarization in MoS_2 monolayers by optical pumping. *Nat. Nanotechnol.* **7**, 490–493 (2012).
10. Y. Li, J. Ludwig, T. Low, A. Chernikov, X. Cui, G. Arefe, Y. D. Kim, A. M. van der Zande, A. Rigosi, H. M. Hill, S. H. Kim, J. Hone, Z. Li, D. Smirnov, T. F. Heinz, *Phys. Rev. Lett.* **113**, 266804 (2014).
11. E. J. Sie, J. W. McIver, Y.-H. Lee, L. Fu, J. Kong, N. Gedik, Valley-selective optical Stark effect in monolayer WS_2. *Nat. Mater.* **14**, 290–294 (2015).
12. D. MacNeill, C. Heikes, K. F. Mak, Z. Anderson, A. Kormányos, V. Zólyomi, J. Park, D. C. Ralph, Breaking of valley degeneracy by magnetic field in monolayer $MoSe_2$. *Phys. Rev. Lett.* **114**, 037401 (2015).
13. A. Srivastava, M. Sidler, A. V. Allain, D. S. Lembke, A. Kis, A. Imamoğlu, Valley Zeeman effect in elementary optical excitations of monolayer WSe_2. *Nat. Phys.* **11**, 141–147 (2015).
14. G. Aivazian, Z. Gong, A. M. Jones, R.-L. Chu, J. Yan, D. G. Mandrus, C. Zhang, D. Cobden, W. Yao, X. Xu, Magnetic control of valley pseudospin in monolayer WSe_2. *Nat. Phys.* **11**, 148–152 (2015).
15. K. F. Mak, K. L. McGill, J. Park, P. L. McEuen, The valley Hall effect in MoS_2 transistors. *Science* **344**, 1489–1492 (2014).
16. M. Z. Maialle, E. A. de Andrada e Silva, L. J. Sham, Exciton spin dynamics in quantum wells. *Phys. Rev. B* **47**, 15776 (1993).
17. K. Hao, G. Moody, F. Wu, C. K. Dass, L. Xu, C.-H. Chen, L. Sun, M.-Y. Li, L.-J. Li, A. H. MacDonald, X. Li, Direct measurement of exciton valley coherence in monolayer WSe_2. *Nat. Phys.* **12**, 677–682 (2016).
18. C. R. Zhu, K. Zhang, M. Glazov, B. Urbaszek, T. Amand, Z. W. Ji, B. L. Liu, X. Marie, Exciton valley dynamics probed by Kerr rotation in WSe_2 monolayers. *Phys. Rev. B* **90**, 161302 (2014).
19. C. Mai, A. Barrette, Y. Yu, Y. G. Semenov, K. W. Kim, L. Cao, K. Gundogdu, Many-body effects in valleytronics: Direct measurement of valley lifetimes in single-layer MoS_2. *Nano Lett.* **14**, 202–206 (2014).
20. H. Yu, G.-B. Liu, P. Gong, X. Xu, W. Yao, Dirac cones and Dirac saddle points of bright excitons in monolayer transition metal dichalcogenides. *Nat. Commun.* **5**, 3876 (2014).

21. L. Yang, N. A. Sinitsyn, W. Chen, J. Yuan, J. Zhang, J. Lou, S. A. Crooker, Long-lived nanosecond spin relaxation and spin coherence of electrons in monolayer MoS_2 and WS_2. *Nat. Phys.* **11**, 830–834 (2015).
22. W.-T. Hsu, Y.-L. Chen, C.-H. Chen, P.-S. Liu, T.-H. Hou, L.-J. Li, W.-H. Chang, Optically initialized robust valley-polarized holes in monolayer WSe_2. *Nat. Commun.* **6**, 8963 (2015).
23. X. Song, S. Xie, K. Kang, J. Park, V. Sih, Long-lived hole spin/valley polarization probed by Kerr rotation in monolayer WSe_2. *Nano Lett.* **16**, 5010–5014 (2016).
24. P. Rivera, K. L. Seyler, H. Yu, J. R. Schaibley, J. Yan, D. G. Mandrus, W. Yao, X. Xu, Valley-polarized exciton dynamics in a 2D semiconductor heterostructure. *Science* **351**, 688–691 (2016).
25. X. Hong, J. Kim, S.-F. Shi, Y. Zhang, C. Jin, Y. Sun, S. Tongay, J. Wu, Y. Zhang, F. Wang, Ultrafast charge transfer in atomically thin MoS_2/WS_2 heterostructures. *Nat. Nanotechnol.* **9**, 682–686 (2014).
26. F. Ceballos, M. Z. Bellus, H.-Y. Chiu, H. Zhao, Ultrafast charge transfer in atomically thin MoS_2/WS_2 heterostructures. *ACS Nano* **8**, 12717–12724 (2014).
27. C. Gong, H. Zhang, W. Wang, L. Colombo, R. M. Wallace, K. Cho, Band alignment of two-dimensional transition metal dichalcogenides: Application in tunnel field effect transistors. *Appl. Phys. Lett.* **103**, 053513 (2013).
28. J. Kang, S. Tongay, J. Zhou, J. Li, J. Wu, Band offsets and heterostructures of two-dimensional semiconductors. *Appl. Phys. Lett.* **102**, 012111 (2013).
29. F. Wang, Y. Zhang, C. Tian, C. Girit, A. Zettl, M. Crommie, Y. R. Shen, Gate-variable optical transitions in graphene. *Science* **320**, 206–209 (2008).
30. Y. Li, A. Chernikov, X. Zhang, A. Rigosi, H. M. Hill, A. M. van der Zande, D. A. Chenet, E.-M. Shih, J. Hone, T. F. Heinz, Measurement of the optical dielectric function of monolayer transition-metal dichalcogenides: MoS_2, $MoSe_2$, WS_2, and WSe_2. *Phys. Rev. B* **90**, 205422 (2014).
31. Z. Chen, S. G. Carter, R. Bratschitsch, S. T. Cundiff, Optical excitation and control of electron spins in semiconductor quantum wells. *Physica E* **42**, 1803–1819 (2010).
32. E. A. Zhukov, D. R. Yakovlev, M. Bayer, M. M. Glazov, E. L. Ivchenko, G. Karczewski, T. Wojtowicz, J. Kossut, Spin coherence of a two-dimensional electron gas induced by resonant excitation of trions and excitons in CdTe/(Cd,Mg)Te quantum wells. *Phys. Rev. B* **76**, 205310 (2007).
33. D. S. Chemla, I. Bar-Joseph, C. Klingshirn, D. A. B. Miller, J. M. Kuo, T. Y. Chang, Optical reading of field-effect transistors by phase-space absorption quenching in a single InGaAs quantum well conducting channel. *Appl. Phys. Lett.* **50**, 585 (1987).
34. A. E. Ruckenstein, S. Schmitt-Rink, R. C. Miller, Infrared and polarization anomalies in the optical spectra of modulation-doped semiconductor quantum-well structures. *Phys. Rev. Lett.* **56**, 504 (1986).
35. F. Rana, P. A. George, J. H. Strait, J. Dawlaty, S. Shivaraman, M. Chandrashekhar, M. G. Spencer, Carrier recombination and generation rates for intravalley and intervalley phonon scattering in graphene. *Phys. Rev. B* **79**, 115447 (2009).
36. B. R. Carvalho, Y. Wang, S. Mignuzzi, D. Roy, M. Terrones, C. Fantini, V. H. Crespi, L. M. Malard, M. A. Pimenta, Intervalley scattering by acoustic phonons in two-dimensional MoS_2 revealed by double-resonance Raman spectroscopy. *Nat. Commun.* **8**, 14670 (2017).
37. L. Wang, I. Meric, P. Y. Huang, Q. Gao, Y. Gao, H. Tran, T. Taniguchi, K. Watanabe, L. M. Campos, D. A. Muller, J. Guo, P. Kim, J. Hone, K. L. Shepard, C. R. Dean, One-dimensional electrical contact to a two-dimensional material. *Science* **342**, 614–617 (2013).
38. N. J. Harmon, *The Ohio State University* (2007).

Acknowledgments

Funding: This work was primarily supported by the U.S. Department of Energy, Office of Science, Office of Basic Energy Sciences, Materials Sciences and Engineering Division under Contract No. DE-AC02-05-CH11231 (Van der Waals Heterostructures program KCWF16). Preparation of hBN single crystals are supported by the Elemental Strategy Initiative conducted by the Ministry of Education, Culture, Sports, Science and Technology, Japan and a Grant-in-Aid for Scientific Research on Innovative Areas, "Science of Atomic Layers," from the Japan Society for the Promotion of Science. S.T. acknowledges the support from NSF Division of Materials Research CAREER award (1552220). **Author contributions:** F.W. and M.F.C. conceived the research. J.K. and C.J. carried out optical measurements. C.J., F.W., and J.K. performed theoretical analysis. J.K., C.J., T.Z., P.L., and S.K. fabricated the van der Waals heterostructures. B.C., H.C., and S.T. grew WSe_2 crystals. K.W. and T.T. grew hBN crystals. All authors discussed the results and wrote the manuscript. **Competing interests:** The authors declare that they have no competing interests. **Data and materials availability:** All data needed to evaluate the conclusions in the paper are present in the paper and/or the Supplementary Materials. Additional data related to this paper may be requested from the authors.

Submitted 16 February 2017
Accepted 20 June 2017
Published 26 July 2017
10.1126/sciadv.1700518

Citation: J. Kim, C. Jin, B. Chen, H. Cai, T. Zhao, P. Lee, S. Kahn, K. Watanabe, T. Taniguchi, S. Tongay, M. F. Crommie, F. Wang, Observation of ultralong valley lifetime in WSe_2/MoS_2 heterostructures. *Sci. Adv.* **3**, e1700518 (2017).